DUPLICATE

Numerical Weather Prediction

Forecasting Research Technical Report No. 383

Parameterisations of the ocean skin effect and implications for satellite-based measurement of sea-surface temperature.

By L.A. Horrocks and B. Candy, T.J. Nightingale,
R.W. Saunders and A. O'Carroll, A.R. Harris

May 2002

© Crown Copyright 2002

Met Office , NWP Division, London Road , Bracknell , Berkshire ,RG12 2SZ, United Kingdom

Forecasting Research
Technical Report No. 383

Parameterisations of the ocean skin effect and implications for satellite-based measurements of sea-surface temperature.

By

L.A. Horrocks and B. Candy,

T.J. Nightingale (Rutherford Appleton Laboratory)

R. W. Saunders and A. O'Carroll,

A.R. Harris (NOAA/NESDIS ORA)

May 2002

The Met Office
NWP Division
Room 344
London Road
Bracknell
RG12 2SZ
United Kingdom

© Crown Copyright 2002

Permission to quote from this paper should be obtained from the above Met Office division

Submitted for publication in *Journal of Geophysical Research – Oceans*

Please notify us if you change your address or no longer wish to receive these publications.

Tel: 44 (0)1344 856245 Fax: 44 (0)1344 854026 email: jsarmstrong@meto.gov.uk

Parameterisations of the ocean skin effect and implications for satellite-based measurement of sea-surface temperature

Lisa A. Horrocks, Brett Candy, Tim J. Nightingale, Roger W. Saunders, Anne O'Carroll and Andrew R. Harris

May 2002

Abstract

Satellite-based retrievals of sea-surface temperature (SST) hold great potential for augmenting and improving existing global climate analyses. However, optimal blending of satellite data with in situ measurements of SST requires an accurate estimate of the temperature difference between radiometric skin and bulk water sampled below the skin. Contemporaneous ship-borne radiometer and in situ measurements of sea surface temperature were obtained during a cruise in the West Pacific and used to define the night time skin-bulk temperature difference. A strong trend of increasing temperature difference with decreasing wind speed was observed. Three published parameterisations of the skin effect have been tested against the ship observations, with excellent agreement achieved by one of these. Good results were also obtained when this scheme was forced by heat fluxes from the Met Office numerical weather prediction global analysis collocated with the observations in space and time. The implementation of a skin effect model in a global satellite data processing system was tested using collocated observations of SST from buoys (bulk) and from ATSR-2 (skin) during 1995–1997. This is a vital step towards integrating accurate satellite retrievals of SST with traditional in situ data sources for climate variability studies.

1. Introduction

Historical data on sea-surface temperature (SST) stretch back to the mid-nineteenth century, providing a vital record of climate variability through this period (e.g. Parker et al., 1995). For the last two decades, satellite observations of SST have been available to augment the existing in situ measurement data. Infrared satellite data have the benefit of consistent spatial coverage, cloud cover permitting, even in regions not covered by ships and buoys. This advantage led to the design of the along-track scanning radiometer (ATSR) series of instruments with the primary purpose of providing highly accurate SST data for climate monitoring.

However, the blending of these two kinds of data for climate analyses is complicated by the fact that satellite-borne sensors infer a temperature related to the ocean radiometric surface skin, i.e., the top few microns in the case of infrared sensors, whereas measurements from ships and buoys sample a bulk surface temperature, typically from depths around 1 m. At the ocean-air interface, a temperature gradient across the molecular boundary layer exists, such that the temperature of the surface skin, T_s is systematically cooler than that of the bulk water, T_b, several cm below (e.g.,

Hasse, 1963; Saunders, 1967; Robinson et al., 1984; Murray et al., 2000). This arises as a result of the size and direction of the vertical heat flux out of the ocean. Heat transfer across this layer occurs by molecular processes of conduction and diffusion. Thus a skin SST derived from satellite measurements may generally be a few tenths of a degree cooler than an equivalent in situ measurement. The exact magnitude of this skin effect, controlled by net heat fluxes and wind speeds, is likely to show seasonal and regional variation, and is not a constant bias. This temperature difference is therefore not negligible given the stringent requirement of 0.1 K per decade stability of observing systems for climate change detection purposes (Allen et al. 1994).

This problem has been circumvented in one approach to SST retrieval. Satellite brightness temperatures in several channels can be regressed against a quality-controlled subset of buoy observations in order to derive a pseudo-bulk temperature, as in the case of AVHRR (e.g., McClain et al. 1985; Walton et al. 1998). However, this assumes a uniform relationship between the skin SST, to which the satellite is sensitive, and the SST measured in situ. This approach introduces uncertainties arising from errors in the in situ data, from spatial and temporal variability below the resolution of collocation, and from lack of representivity in regions without in situ data. An alternative approach to derivation of satellite SSTs is to retrieve the radiometric skin temperature directly, based on accurate radiative-transfer modelling (e.g., Llewellyn-Jones et al. 1984; Závody et al. 1995). Either the satellite (skin) or in situ (bulk) data can then be converted, using a physical parameterisation for the ocean skin, to achieve equivalence between the two observation types. From the perspective of augmenting the existing climatological archive of SST data, the conversion of satellite SST to an equivalent bulk temperature is desirable, both to achieve parity with traditional measurements, and because the bulk temperature is more representative of the ocean's store of heat than is the skin (e.g., Harris et al 1998).

Numerous parameterisations for the cool ocean skin exist, and these have generally been based on one of two different foundations. Using dimensional arguments, Saunders (1967) presented a physical model for the skin by assuming heat transfer through a viscous boundary layer at a rigid surface, with the skin defined as the thickness in which heat transfer by molecular conduction dominates. Beneath the skin, two regimes may be envisaged, depending on whether heat transport is controlled by shear-generated turbulence (forced convection) or by buoyancy-generated turbulence (free convection). The temperature difference in the forced regime, ΔT across the skin (defined as bulk SST minus skin SST) is given by

$$\Delta T = \frac{\lambda Q \nu}{k u_*}, \qquad (1)$$

where Q is the net heat flux out of the ocean, ν is the kinematic viscosity of seawater, k is the thermal conductivity of seawater, u_* is the friction velocity in the water, and λ is an empirical proportionality constant (known as the Saunders coefficient). This model applies only to the forced convection regime: since u_* is closely related to wind speed, the value of ΔT tends to ∞ as the wind speed approaches zero. In the free convection regime, ΔT is independent of wind speed. Fairall et al (1996a) extended the descriptions laid down by Saunders, providing a combined

expression for ΔT, applicable at all wind speeds, that achieved a smooth transition between the two regimes.

An alternative approach to the problem is provided by surface renewal theory, and Soloviev and Schlüssel (1994) based their parameterisation on earlier work in this area (e.g., Liu and Businger 1975; Liu et al. 1979). Wick et al. (1996) showed that existing models for the skin-bulk temperature difference (including those following the standard Saunders treatment) in the shear-driven regime could be derived from surface renewal theory with slightly differing definitions of the turbulent kinetic energy dissipation rate. True surface renewal theory models predict an additional Reynolds number proportionality in the ΔT-dependence rather than a simple dependence on Q/u_* as originally proposed by Saunders.

Shipborne radiometer data have often been used in validation of satellite-derived SSTs (e.g., Barton et al. 1995; Donlon and Robinson 1997; Kearns et al. 2000; Minnett et al. 2001). These data, combined with in situ measurements of bulk SST, can also be used to investigate skin-bulk temperature differences and to test methods for reconciling the two measurement types. Kent et al. (1996) compared the performance of the models suggested by Saunders (1967), Soloviev and Schlüssel (1994), Schlüssel et al (1990) and Hasse (1971), using shipborne radiometer data from the region around the Azores. These authors reported that in the 3–7 ms^{-1} wind speed range, the Saunders model best reproduced the observed skin effect variability.

In this paper, we use data collected on a research cruise in the West Pacific (between 0 and 35° N), during June–July 1999. We first characterise the skin-bulk temperature difference revealed by the ship data. Second, we use these data to compare three published skin effect models chosen as representative of the two theoretical approaches outlined above. We also investigate the impact of using flux data from NWP model analysis fields, rather than in situ meteorological measurements, in the parameterisations. We then use observations from ATSR-2, collocated with buoy data, to test the implementation of a skin effect model within a processing scheme for satellite SSTs. Finally, we discuss implications of this study for the future use of satellite data in SST analyses for climate research.

2. Ship Data and Methodology

Under the U.S. Department of Energy's Atmospheric Radiation Measurement (ARM) program, the Japan Marine Science and Technology Center (JAMSTEC) research ship, the *R/V Mirai* was deployed in the tropical Western Pacific in June–July 1999 for the Nauru99 campaign. A scanning infrared sea surface temperature radiometer (SISTeR) was mounted on the railings of the lower foremast platform of the *R/V Mirai*, to measure skin SST to accuracies better than ±0.05 K. The SISTeR is a compact and flexible chopped self-calibrating infrared filter radiometer, designed for research in a marine environment (e.g., Donlon and Nightingale, 2000; Donlon et al., 2002). It was developed expressly to validate ATSR-2, and contains filters at 3.7, 10.8 and 12.0 μm built to ATSR-2 specifications. Two internal blackbodies maintained at different temperatures act as references for the external radiance measurements, and the SISTeR calibration was checked at the beginning of the cruise against a CASOTS blackbody cavity (Donlon et al. 1999). Skin SSTs were calculated from the 10.8 μm channel radiances sampled every 0.8 s, corrected for a small reflected sky radiance term. All data were collected into 10-minute bin means and quality controlled to exclude erroneous measurements, such as those obtained while the ship was stationary, or when the instrumental field of view was obstructed.

Bulk SST was sampled with an estimated accuracy of ±0.001 K using a Sea-Bird Electronics temperature sensor (SBE 3S) located at a depth of 4.5 m at the sea-water inlet into the ship's bow thruster room. Air and dew point temperatures were measured with pairs of Koshin FT thermometers and DW-1 dew point meters located on either side of the ship at an elevation of 18 m, and data were selected from those exposed to the prevailing wind. Wind speed and direction were recorded at an elevation of 24 m with a Koshin KE-500 anemometer. The downwelling short- and long-wave radiative fluxes were recorded at 28 m with an EIKO MS-801 pyranometer and an EIKO MS-202 pyrgeometer, respectively. For the majority of the cruise, the sky contained some cloud, either in the form of cumulus cells which sometimes produced showers, or as cirrus. No data were collected from the SISTeR during rainy periods.

Figure 1 shows the location of observations collected during the cruise. Wind speed data were converted to equivalent 10-m height winds using a logarithmic scaling for easier comparison with standard measurements and NWP model wind fields. Latent and sensible heat fluxes were computed from the meteorological data using bulk formulae, following Fairall et al. (1996b) and Smith (1988), and the net long-wave heat flux was computed from the measured downwelling flux and skin SST). The net non-solar heat flux out of the ocean, Q, was then the sum of the latent, sensible and net long-wave heat fluxes.

In order to focus on the skin-bulk temperature difference arising from skin effect processes alone, only data collected at night have been used: this selection ensures that complications arising from diurnal warming and thermal stratification are avoided, and that the models are tested under the conditions for which they were developed. A few observations for which the bulk SST was cooler than the skin SST at night were rejected since they also recorded anomalously cool bulk SST. After filtering, the night time data set contained 1210 observations of ΔT, wind speed and heat flux.

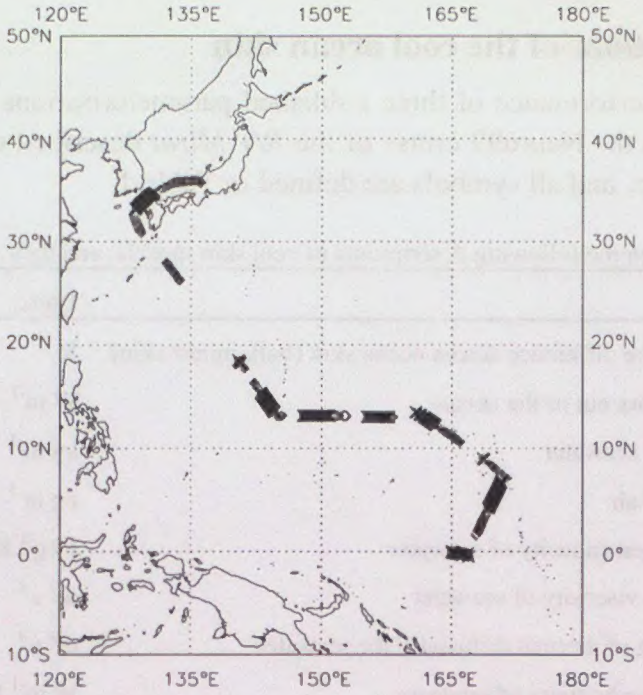

Figure 1: Location of valid measurements collected during the June–July 1999 cruise of the *R/V Mirai* in the western Pacific. The night time subset is plotted in black.

The models described below involve a friction velocity term. This refers to the efficiency with which the wind generates shear turbulence in the ocean below. The rate of dissipation of turbulent kinetic energy, ε, scales as u_*^3/z for turbulence generated by pure shear, where z is depth and measured positive downward from the ocean surface. The value of u_* can be derived iteratively from measurements of wind speed at a known height above the surface, by assuming a logarithmic wind speed profile and a roughness length-friction velocity relationship, such as that of Pierson (1978): this approach was taken for the in situ wind speed measurements. Alternatively, u_* can be calculated directly from wind-mixing energy flux (F_{wme}) fields generated operationally by an NWP model, such as the Met Office Unified Model (Cullen 1993). F_{wme} is the rate of production of turbulent kinetic energy per unit area in the sea surface layer by the wind stress at the air-sea interface. Under sea-ice free conditions, F_{wme} and u_* are related by (2) (e.g., Smith and Williams 2000):

$$u_* = \left(\frac{F_{wme}}{\rho} \right)^{1/3} , \qquad (2)$$

where ρ is the density of seawater. Friction velocities in the atmosphere and ocean immediately above and below the interface (u_{*a} and u_*, respectively) are related by assuming that the stresses on both sides of the ocean-air interface are balanced, so that

$$\rho u_*^2 = \rho_a u_{*a}^2 . \qquad (3)$$

where ρ_a is the density of the air above the interface.

3. Parameterisations of the cool ocean skin

We assess the performance of three published parameterisations of the skin effect, using the data from the Nauru99 cruise of the *R/V Mirai* described above. The models are summarised here, and all symbols are defined in Table 1.

Table 1: Symbols used in the following descriptions of cool skin models, and their meanings.

Symbol	Meaning	Units
ΔT	temperature difference across ocean skin (bulk minus skin)	K
Q	net heat flux out of the ocean	$W\ m^{-2}$
ρ	density of seawater	$kg\ m^{-3}$
ρ_a	density of air	$kg\ m^{-3}$
c_p	specific heat capacity of seawater	$J\ kg^{-1}\ K^{-1}$
ν	kinematic viscosity of seawater	$m^2\ s^{-1}$
κ	coefficient of thermal diffusivity for seawater	$m^2\ s^{-1}$
k	thermal conductivity of seawater	$W\ m^{-1}\ K^{-1}$
α	coefficient of thermal expansion for seawater	K^{-1}
u_*	friction velocity in the water	$m\ s^{-1}$
u_{*a}	friction velocity in the atmosphere	$m\ s^{-1}$
z_o	surface roughness length	m
g	gravitational acceleration	$m\ s^{-2}$
Rf	Richardson number	
Pr	Prandtl number	
Ke	Keulegan number	
λ	Saunders coefficient	
A	empirical convection coefficient used by FA	
Λ_o	proportionality coefficient used by SS	
C_{sh}	shear proportionality constant in WI	
C_{conv}	convective proportionality constant in WI	

3.1 Fairall et al (1996a)

Fairall et al (1996a, hereafter FA) built on earlier work by Saunders (1967). Under the standard Saunders treatment, the regime at low windspeeds, under which convectively-driven turbulence dominates, was ignored. FA's extension was to treat both shear- and convectively-driven turbulence together through their contribution to the near-surface turbulent kinetic energy dissipation rate. This dissipation rate directly affects the cool skin layer thickness, and so the effect can be incorporated via a buoyancy-dependent λ coefficient. Appropriate values of between 4 and 8 for a fixed λ were suggested in numerous earlier studies, but FA provided a parameterisation in which λ was a function of heat flux and friction velocity.

$$\lambda = \lambda_0 \left[1 + \left(\frac{\lambda_o^4 A^3 Q g \alpha \rho c_p \nu^3}{u_{*a}^4 (\rho_a/\rho)^2 k^2} \right)^{3/4} \right]^{-1/3} , \qquad (4)$$

where g is gravitational acceleration, α is the coefficient for thermal expansion of seawater, ρ and ρ_a are densities of seawater and air, respectively, and c_p is the specific heat capacity of seawater. A is an empirical convection coefficient, defined by consideration of the convectively-generated turbulence regime, with a value of around 0.23 suggested by FA (cf. Saunders, 1967, suggested 0.2). FA replace Q with a virtual surface cooling term which takes into account the buoyancy effects of evaporation-induced salinity changes: we approximate here with the net non-solar heat flux since salinity effects will be strongest in the free convection regime, where also latent heat fluxes are lowest and our approximation most valid. λ_0 is equivalent to the value of λ used in a standard Saunders treatment, away from low wind speeds. Thus, the model follows the Saunders forced convection scheme under shear-driven turbulence in the high windspeed regimes, with λ tending to the λ_0 value, suggested to be around 6 by FA. At lower wind speeds, the value of λ decreases as the contribution from shear reduces. ΔT is calculated using the Saunders equation with the FA definition of λ. Following (3), $u_{*a}{}^4(\rho_a/\rho)^2$ can be replaced by $u_*{}^4$ and (4) becomes

$$\lambda = \lambda_0 \left[1 + \left(\frac{\lambda_0^4 A^3 Q g \alpha \rho c_p \nu^3}{u_*^4 k^2} \right)^{3/4} \right]^{-1/3} . \qquad (5)$$

FA also considered the effect of solar heating within the skin layer, which would act to reduce the normal cooling effect at the ocean surface. Their results implied that, for wind speeds below ~1 m s^{-1}, the solar flux absorbed within the expected thickness of a cool skin may exceed the total cooling at the interface arising from net long wave heat output from the ocean, irrespective of any additional diurnal warming. This effect, which would be greater in the tropics than at high latitudes, is not explicitly included in (5): for the night time data considered here, this extension is not needed.

3.2 Soloviev and Schlüssel (1994)

Soloviev and Schlüssel (1994, hereafter SS) built on surface renewal theory, in which the surface Richardson number controls the transition from convective instability to wind-induced instability. Three key parameters were used by SS: the surface Richardson number, Rf (which controls the transition from free to forced convection in the near-surface layer), the Prandtl number, Pr, and the Keulegan number, Ke (which controls the transition from rollers to long-wave breaking in the near-surface ocean), where

$$Rf = -\frac{\alpha g Q \nu}{u_*^4 c_p \rho} , \qquad (6)$$

$$\mathrm{Pr} = \frac{\nu}{\kappa} , \qquad (7)$$

$$\mathrm{Ke} = \frac{u_*^3}{g\nu} \quad . \qquad (8)$$

Symbols in (6) to (8) have the same meanings as previously given, and κ is the coefficient for thermal diffusivity of seawater. SS indicated that appropriate critical values for Rf and Ke were $Rf_{cr} = -1.5 \times 10^{-4}$ and $\mathrm{Ke_{cr}} = 0.18$. These parameters were combined to provide an estimate for the temperature difference across the cool skin:

$$\Delta T = \Lambda_0 \frac{Q}{c_p \rho u_*} \mathrm{Pr}^{1/2} \left(1 + \frac{Rf_0}{Rf_{cr}}\right)^{-1/4} \left(1 + \frac{\mathrm{Ke}}{\mathrm{Ke_{cr}}}\right)^{1/2} , \qquad (9)$$

where Λ_0 is a dimensionless proportionality constant, given the value of 13.3 by SS, based on previous work.

3.3 Wick et al (1996)

Wick et al (1996, hereafter WI) developed a new model for the skin-bulk temperature difference following an extensive comparison of some existing models against two sets of night time ship data. In their study, this new model performed as well as or better than the others that they tested. They combined equations derived by Liu et al (1975), Liu and Businger (1979) and SS for the different regimes (shear-driven and free convection), with the transition governed by the surface Richardson number, to form (10):

$$\Delta T = \frac{Q}{\rho c_p \kappa^{1/2}} \left\{ C_{sh} \left(\frac{\nu z_o}{u_*^3}\right)^{1/2} + \left[C_{conv} \left(\frac{\nu \rho_w c_p}{\alpha g Q}\right)^{1/2} - C_{sh} \left(\frac{\nu z_o}{u_*^3}\right)^{1/2} \right] e^{-(Rf_{cr}/Rf_o)} \right\}^{1/2} . \quad (10)$$

The shear and convective proportionality constants, C_{sh} and C_{conv}, respectively, were tuned to the characteristics of each data set. We generate values for our data in the analysis below.

4. Observations and model results

4.1 Summary of the ship data

Observed ΔT was calculated as bulk SST minus skin SST. These data are plotted as a function of the 10-m wind speed in Figure 2, showing both the full cruise data set and the night time subset used in this study. The wide range of observed ΔT at low wind speeds in Figure 2a is likely related to complications arising from diurnal warming and solar absorption in the skin layer: this scatter was entirely removed in the night time subset (Figure 2b). The night time data showed a strong trend towards larger ΔT at the lowest windspeeds, in common with many previous observations (e.g., Wick et al., 1996; Fairall et al., 1996a; Murray et al., 2000; Donlon et al., 2002).

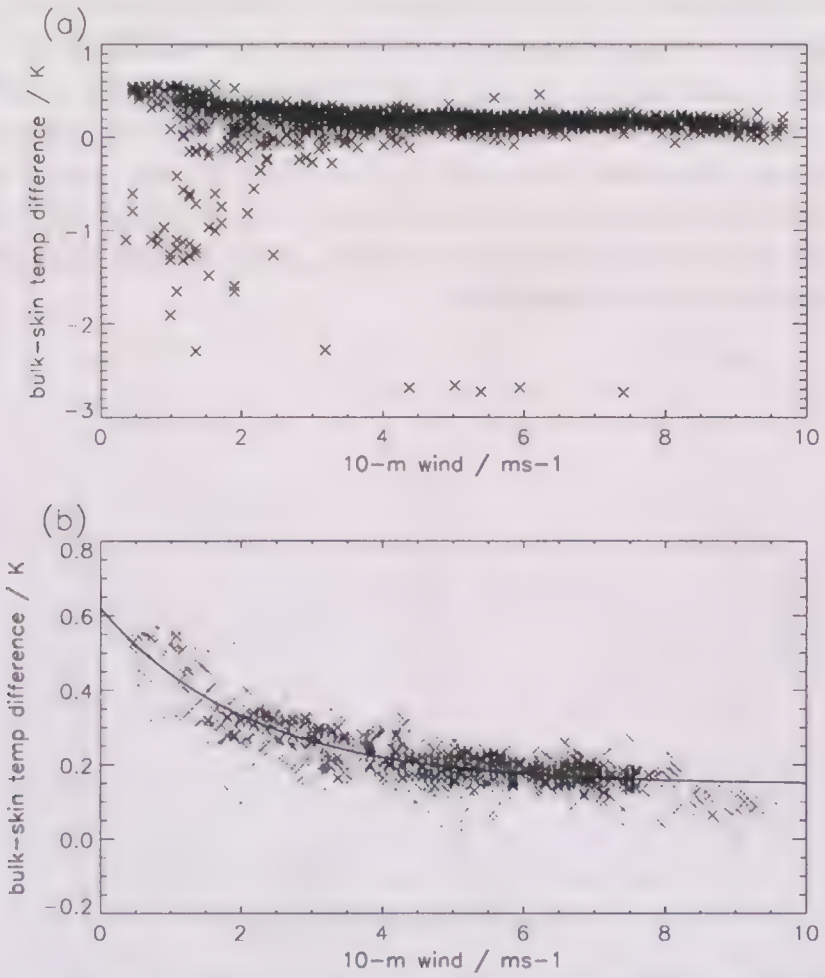

Figure 2: Bulk minus skin SST difference plotted against measured wind speeds, corrected to a standard 10-m height. (a) the full dataset: notice the considerable scatter at low wind speeds, related to complications from diurnal warming. (b) night time SST data, plotted on an expanded axis, show a tight trend with wind speed. The curve is an empirical best fit to the data; see text for description.

We assumed an exponential wind-speed dependence, and used a non-linear least squares routine with the data to fit the coefficients in an empirical function:

$$\Delta T = a + b\exp\left(-\frac{u}{u_o}\right), \qquad (11)$$

where u is the 10-m wind speed, and a, b and u_o were found to have values of 0.15, 0.47 and 2.1, respectively. This function has been plotted in Figure 2b. Donlon et al. (2002) obtained a similar function (their equation 2) for night time data, which consisted of measurements from six cruises, including the data used here. However, for that larger dataset, the relationship between wind speed and ΔT was well-defined only for wind speeds above 3 ms^{-1}. The greater scatter associated with data from a larger range of locations and latitudes is most likely related to the greater range of net heat fluxes relevant to the observations. Despite these differences, there is good agreement between (11) and the function suggested by Donlon et al.: we derive a scale wind speed, u_o, less than the 3.7 ms^{-1} they suggest, but both functions asymptote at high wind speed to a ΔT of ~0.15 K.

Figure 3 is a histogram showing the frequency distribution of observed ΔT, binned at 0.02 K intervals. For these data, the mean observed ΔT was 0.22 K (σ = 0.084 K), which is similar to some reports of ΔT for the W. Pacific (Webster et al. 1996; Murray et al. 2000), but slightly less than some others (e.g., Fairall et al. 1996a). For wind speeds above 6 ms^{-1}, the mean ΔT was 0.17 K (σ = 0.04 K), the same as the average value in this wind speed range calculated by Donlon et al. (2002) for their broader data base. The small standard deviations reflect the quality of these SST measurements, and the restricted range of ambient conditions.

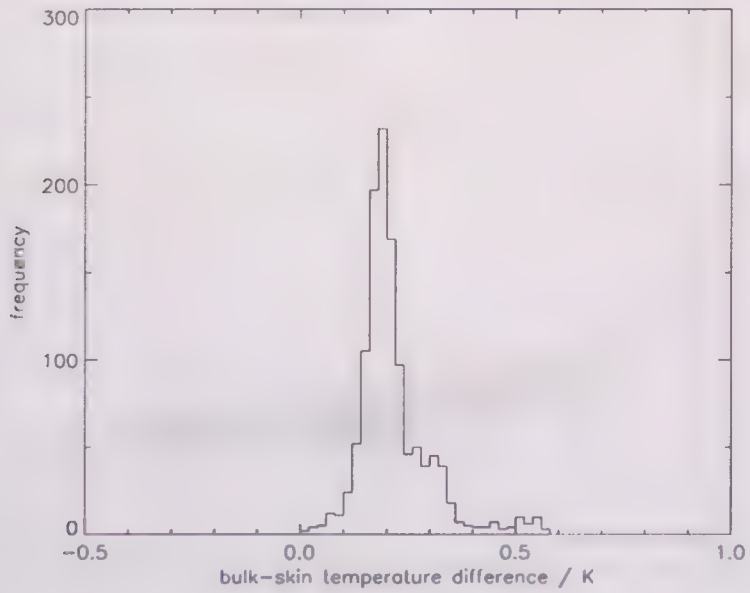

Figure 3: Frequency distribution of night time ΔT, for data in 0.02 K intervals.

4.2 Predictions of the parameterisations using in situ fluxes

To assess the performance of the parameterisations introduced in Section 3, the heat fluxes and friction velocities associated with each pair of skin and bulk SSTs were used to predict ΔT following the equations presented above.

The FA model predicted values of ΔT which corresponded well with the observed values across the whole wind speed range (Figures 4a and b). The best correlation was achieved by setting the coefficient, λ_o, to 4.6, which is lower than some values suggested for the λ parameter in standard Saunders schemes (c.f. FA estimate a value

of 6). We noted earlier that values of ΔT measured during this cruise were smaller than in some other studies: a smaller value of λ_o is therefore required in the model.

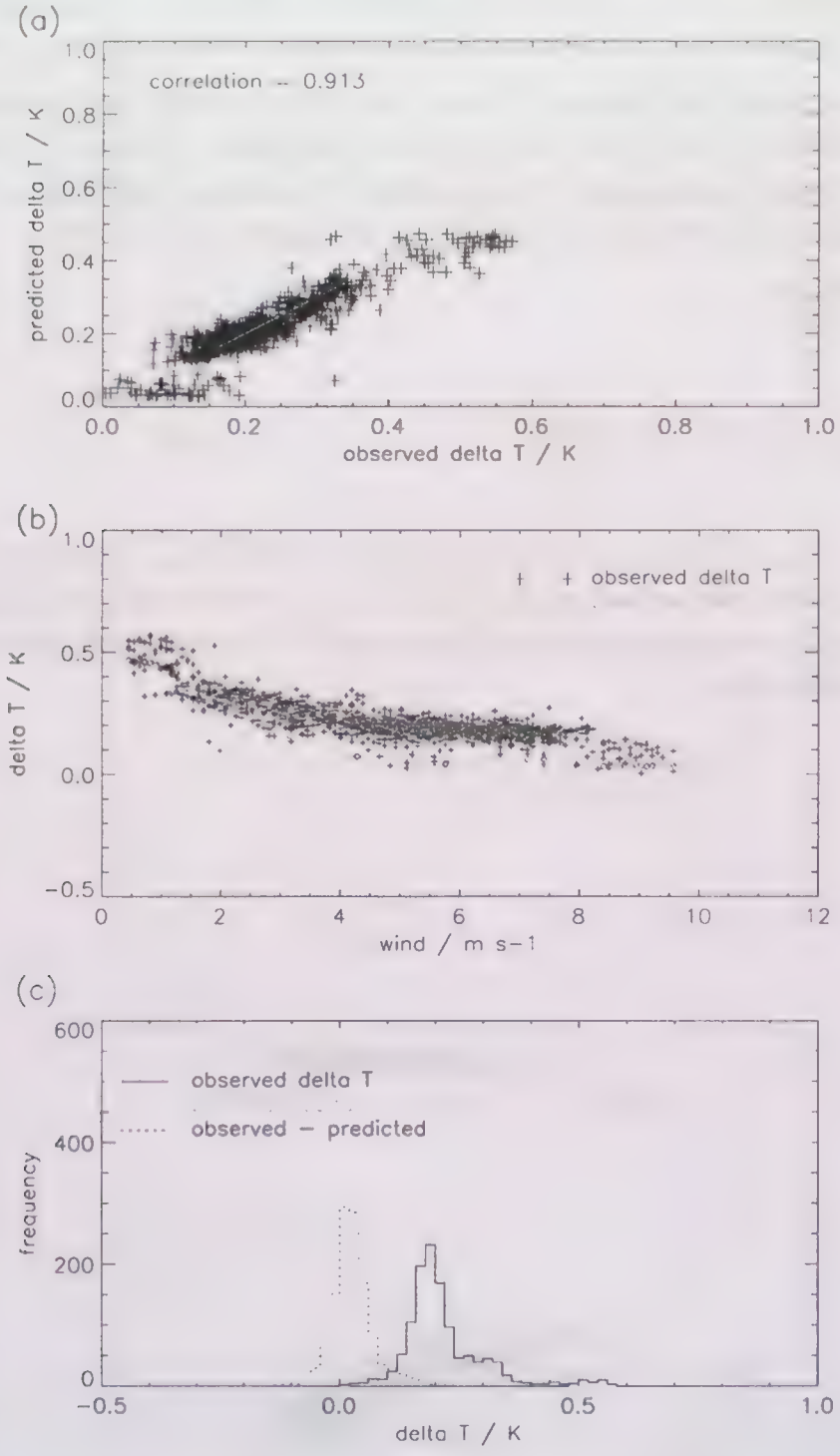

Figure 4: Results of model predictions of ΔT using FA scheme, with λ_o of 4.6. (a) predicted ΔT plotted against observed ΔT, in K; (b) ΔT plotted as a function of windspeed, observed values as black crosses and predicted values as grey open symbols; (c) histogram showing ΔT binned according to windspeed, with observed in solid black line, predicted in solid grey line, and δT_{o-p} in dotted black line.

The skill of the model is seen from Figure 4c, showing frequency distributions of the observed and predicted ΔT (as in Figure 3). The mean predicted value of ΔT was 0.21 K, ($\sigma = 0.074$ K) close to the mean of the observations (0.22 K). Also shown is the

difference between observed and predicted values, hereafter referred to as $\delta T_{o\text{-}p}$. The mean $\delta T_{o\text{-}p}$ was 0.027 K, with a standard deviation of 0.045, compared to the standard deviation of 0.084 K of the observed ΔT. The 46 % reduction in standard deviation indicates the improvement achieved by this scheme over a fixed value skin correction.

For application of the model by SS, the critical *Rf*, Pr and Ke were all fixed at the values suggested by them. The value of the proportionality constant, Λ_o, in (9) was defined by a linear least squares fit of a product G, containing the observed ΔT, to a product H, containing the critical parameters on the right-hand side of (9):

$$G = \frac{\Delta T c_p \rho u_*}{Q} , \tag{12}$$

$$H = \mathrm{Pr}^{1/2}\left(1+\frac{Rf_0}{Rf_{cr}}\right)^{-1/4}\left(1+\frac{\mathrm{Ke}}{\mathrm{Ke}_{cr}}\right)^{1/2} . \tag{13}$$

The data are not well approximated by a linear model (Figure 5), but the retrieved value for Λ_o using this method was 11.7. This is less than the value of 13.3 suggested by SS, which is unsurprising given the higher mean ΔT for the experimental data they used in their derivation.

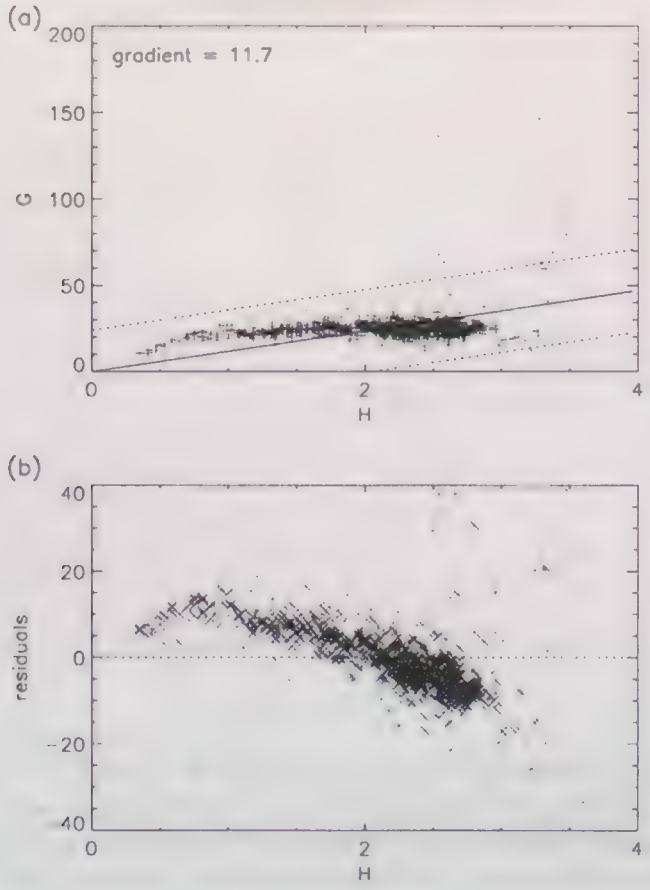

Figure 5: (a) Linear regression of G against H, as defined in (12) and (13), to determine the value for Λ_o in (9) for the application of the SS scheme; (b) residuals from the regression in (a).

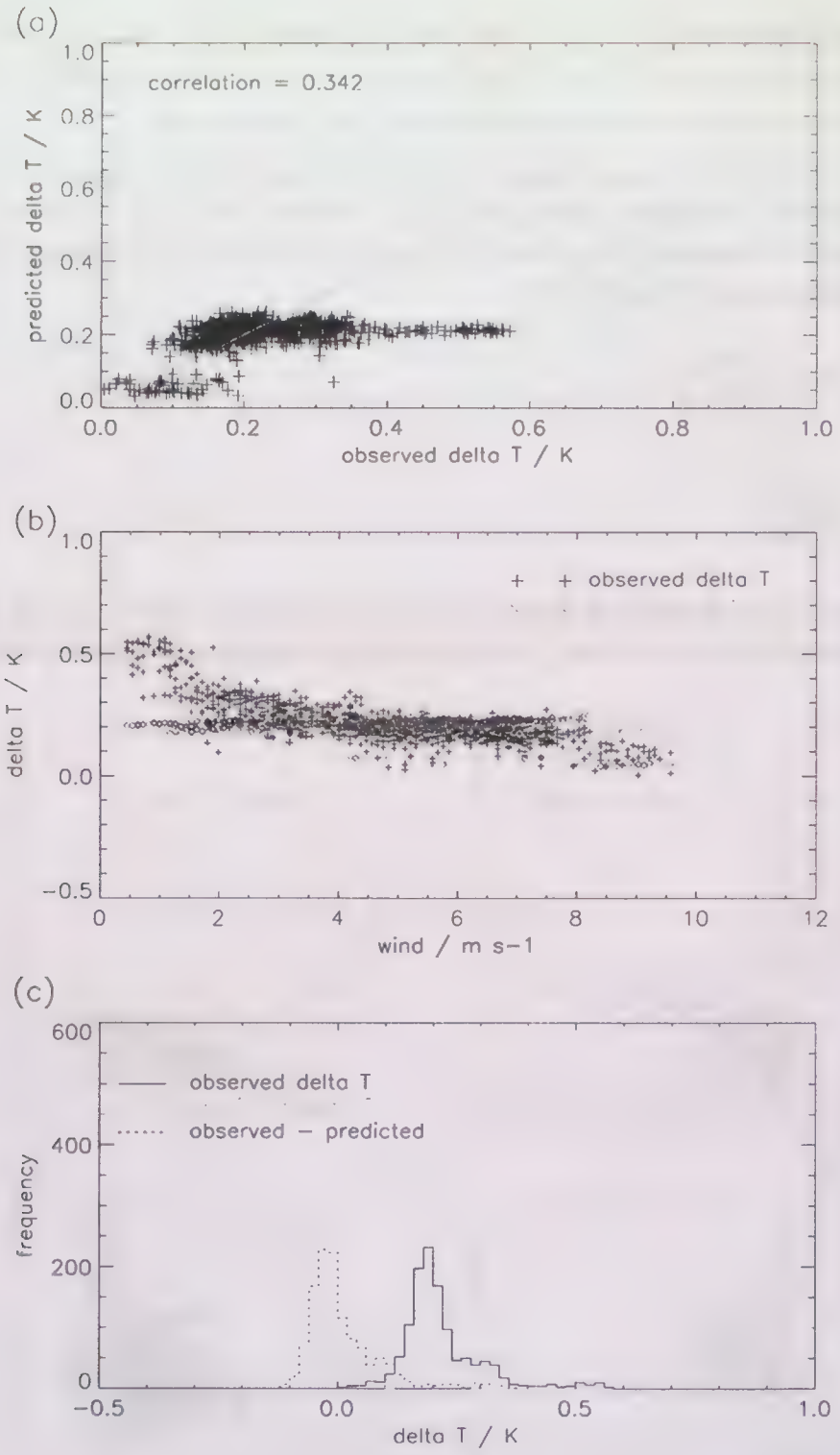

Figure 6: Results of model predictions of ΔT using SS scheme. (a) predicted ΔT plotted against observed ΔT, in K; (b) ΔT plotted as a function of windspeed, observed values as black crosses and predicted values as grey open symbols; (c) histogram showing ΔT binned according to windspeed, with observed in solid black line, predicted in solid grey line, and δT_{o-p} in dotted black line.

The correlation of predicted and observed ΔT is poor (Figure 6a), resulting from the fact that this model fails to reproduce the trend of ΔT against windspeed (Figure 6b). The shape of the frequency distribution indicates that ~80 % of the predicted values for ΔT were in the range 0.18 to 0.22 K: the mean was 0.20 K (σ = 0.038), similar to the

mean of the observations, since Λ_o was tuned to achieve this. However, this scheme failed to model the observed range of ΔT, and the standard deviation of $\delta T_{o\text{-}p}$ (0.080 K) was little changed from the standard deviation of the observations.

For the WI model, the appropriate value for the shear proportionality constant, C_{sh}, was determined following the procedure outlined by WI. Values for the experimentally-determined (tr_{obs}) and theoretically-predicted (tr_{pr}) renewal timescales were computed using (14) and (15):

$$tr_{obs} = \kappa \left(\frac{\Delta T \rho c_p}{Q} \right)^2 \tag{14}$$

$$tr_{pr} = \left(\frac{\nu z_o}{u_*^3} \right)^{1/2} \tag{15}$$

The results of a linear least squares regression between tr_{obs} and tr_{pr} are shown in Figure 7. To obtain the value for C_{sh}, the gradient of the regression line for data in the

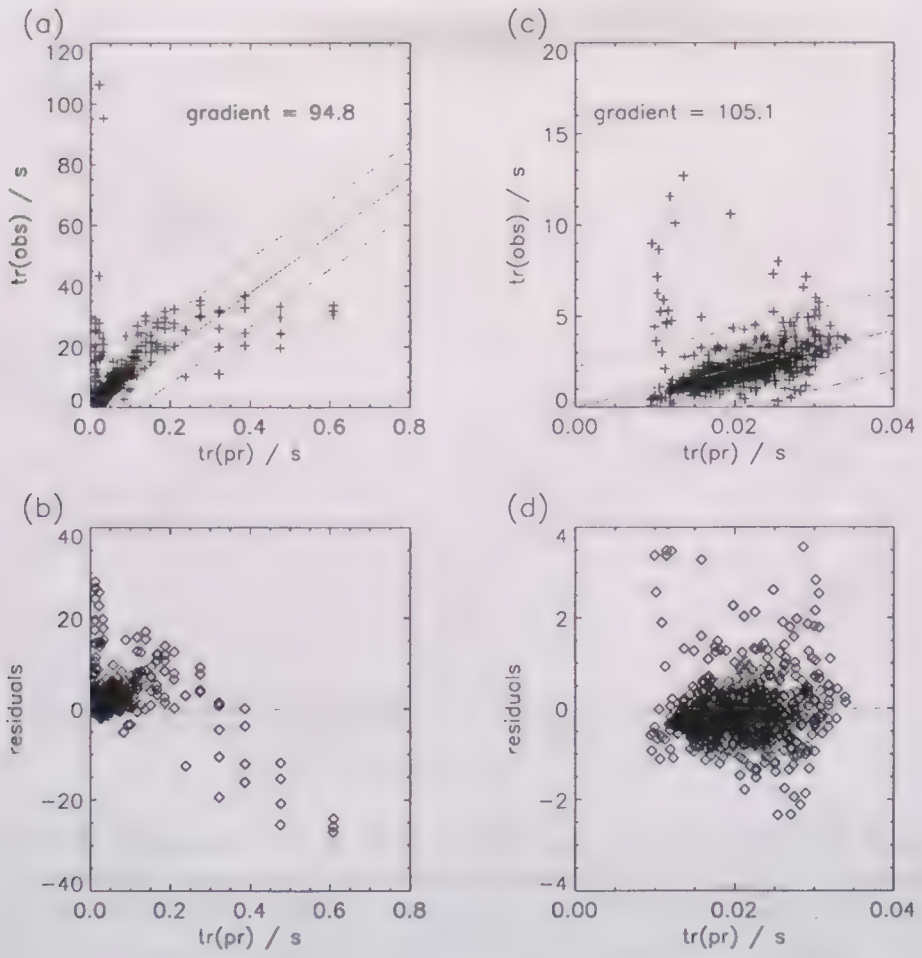

Figure 7: Comparison between experimentally-derived renewal timescale estimates with theoretical predictions, following WI. (a) for all data, with residuals in (b); (c) data for which $|Rf_o| < |Rf_{cr}|$, with residuals in (d). The solid line in (a) and (c) shows the best fit achieved through linear regression: gradients of the fits are marked.

shear regime (i.e., where $|Rf_o| < |Rf_{cr}|$) was used (Figure 7c). The value for the convective proportionality constant, C_{conv}, was calculated from the relationship between C_{sh}, C_{conv}, and Rf_{cr} cited by WI:

$$Rf_{cr} = -(C_{conv}/C_{sh})^2 \qquad (16)$$

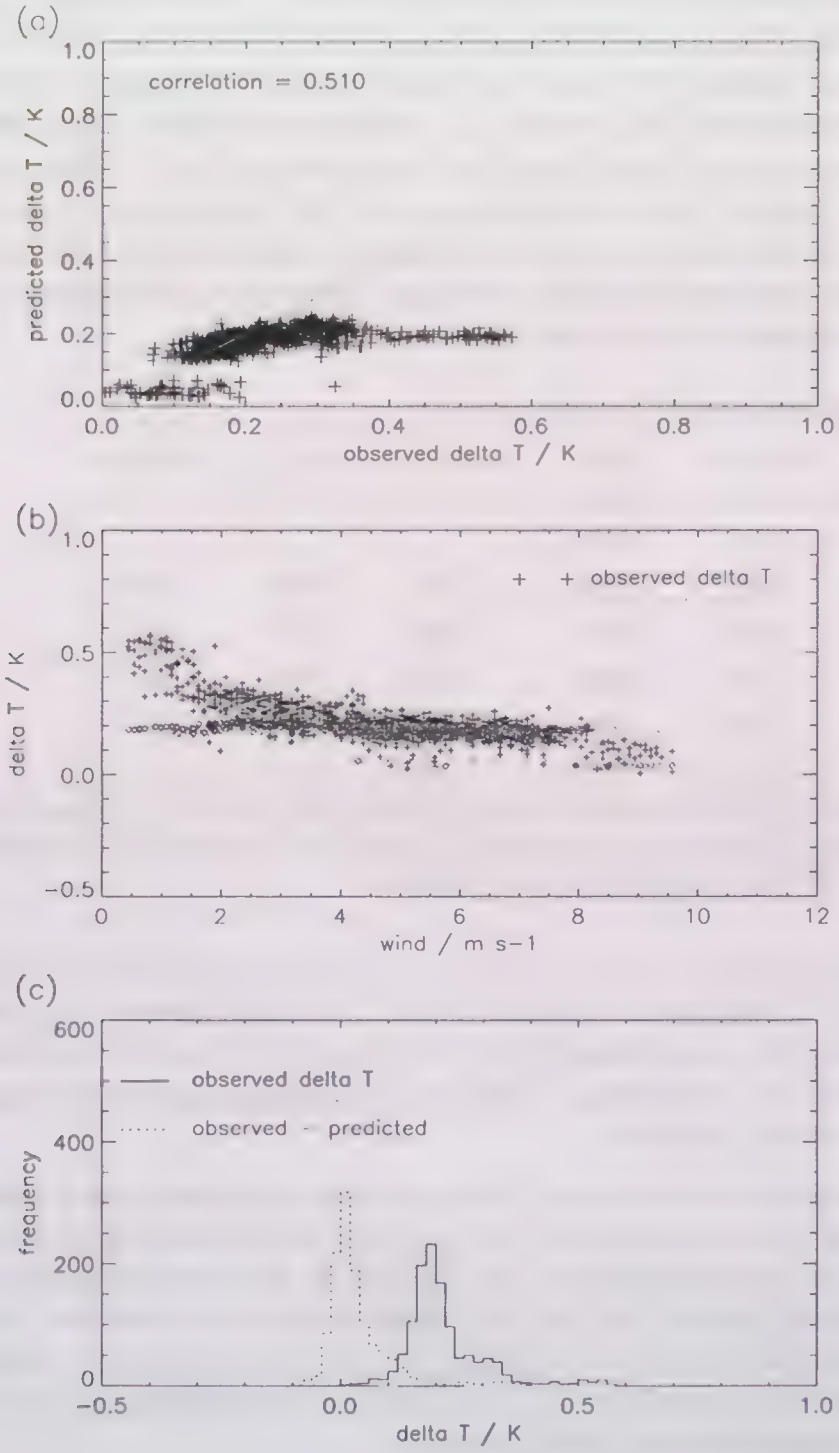

Figure 8: Results of model predictions of ΔT using WI scheme. (a) predicted ΔT plotted against observed ΔT, in K; (b) ΔT plotted as a function of windspeed, observed values as black crosses and predicted values as grey open symbols; (c) histogram showing ΔT binned according to windspeed, with observed in solid black line, predicted in solid grey line, and δT_{o-p} in dotted black line.

The results in Figure 8 were from calculations for which Rf_{cr} was set at -1.6×10^{-4}: in practice, it made little difference whether the value was chosen to be -1.5×10^{-4}, as accepted by SS, or -1.6×10^{-4}, as recommended by WI. This model gave a similar performance to that of SS, as might be expected for parameterisations that are so closely related.

All of the model results are summarised in Table 2. Also shown is the correction obtained using the exponential relationship given in (11). It is clear that the FA model produced the closest match across the whole range of ΔT measured on the Nauru cruise. The models based most closely on surface renewal theory, SS and WI, failed to predict the increase of ΔT observed at low wind speeds (Figure 2), although both could be tuned to produce the correct mean value of ΔT. Consequently, the width of the histograms for model error was greater in these two models than for FA. Under the FA approach, the skin-bulk temperature difference is governed by the thickness of the skin layer, which is predicted to increase at low wind speeds.

Table 2: Summary of the skin effect model predictions.

	Mean ΔT / K	$\sigma(\Delta T)$ / K	Mean δT_{o-p} / K	$\sigma(\delta T_{o-p})$ / K	Correlation
Observed	0.216	0.084			
Exponential	0.216	0.072	< 0.001	0.043	0.86
FA	0.212	0.074	0.027	0.045	0.92
SS	0.204	0.038	0.012	0.080	0.34
WI	0.178	0.036	0.038	0.073	0.51
FA (NWP)	0.211	0.062	0.005	0.050	0.80

Notes: Mean ΔT represents bulk minus skin temperature difference. Mean δT_{o-p} represents observed minus predicted ΔT difference. The correlation value was calculated as the simple product-moment correlation coefficient between observed and predicted ΔT.

The results for the surface renewal theory models here are similar to those obtained by Kent et al (1996) from their application of SS to ship-borne data collected in the region around the Azores. Although they did not test FA, Kent et al found that for wind speeds of 3–7 ms^{-1}, the original Saunders (1967) model performed better than the alternative schemes they tried.

The empirical ΔT–wind speed relationship derived for these data provided a good fit because a strong correlation between net heat flux and wind speed existed in this spatially- and temporally-limited study (Figure 9). For data extending to different regions, and for different seasons, the apparent dependence of net heat flux on wind speed may not hold, and the exponential fit in (11) may break down. The skin effect parameterisations include net heat flux and wind speed independently and should therefore be appropriate for global application.

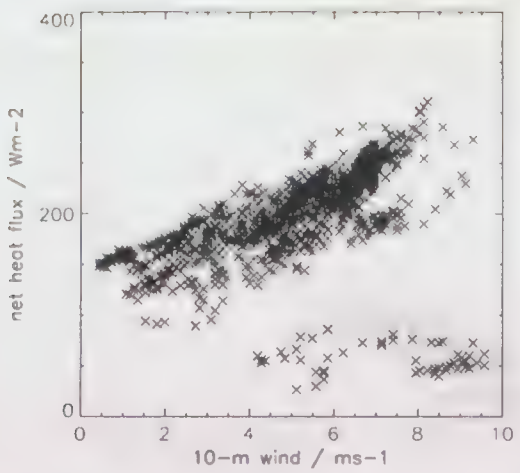

Figure 9: Relationship between observed net heat flux and 10-m wind speed for the cruise data.

4.3 Prediction of the FA scheme using NWP model flux data

Since one application for ocean skin parameterisations is conversion of satellite-derived skin SST to bulk SST for near-real time operational use (e.g., Harris et al. 1998), they must be able to make accurate predictions when supplied with operational heat flux and wind fields from an NWP model analysis rather than relying on meteorological data collected in situ. We used heat flux and wind-mixing energy flux data from Met Office Unified Model global NWP analyses, matched to the time and location of each set of skin and bulk SST observations. These model fluxes were 6-hourly averages, as this was the temporal resolution available from the Met Office model for operational use in a satellite data correction scheme. For these calculations, u_* was computed directly from the model wind-mixing energy flux field using (2). The value for λ_o was kept as 4.6, as derived for the in situ data, above, but in order to obtain a good match to the observed ΔT, a systematic offset of 0.04 K was subtracted from the new predicted values of ΔT. Results (with this offset applied) are shown in Figure 10, which should be compared to Figure 4.

The correlation between modelled and observed ΔT (Figure 10a) was less than that achieved when the in situ meteorological data were used, but the trend of ΔT was still captured strikingly well over most of the wind speed range. Considerable model skill was retained: the standard deviation of δT_{o-p} was 0.050 K compared with the standard deviation of the observations at 0.084 K.

The 0.04 K offset applied to the model ΔT arises as a result of using NWP fluxes in place of the in situ measurements. A notable difference in the performance of the FA scheme in this respect was at extremes of the wind speed range (Figure 10b). When the model was forced with in situ fluxes (Figure 4b), it captured the trend of ΔT with wind speed very closely throughout the entire wind speed range. When the model was forced with NWP fluxes, predicted ΔT was lower than observed at low wind speeds and higher than observed at high wind speeds. This is unsurprising, given that the NWP model wind-mixing energy flux field is averaged both temporally (over a 6-hour analysis window) and spatially, since values at specific locations were obtained by linear interpolation from the 50 km resolution model grid.

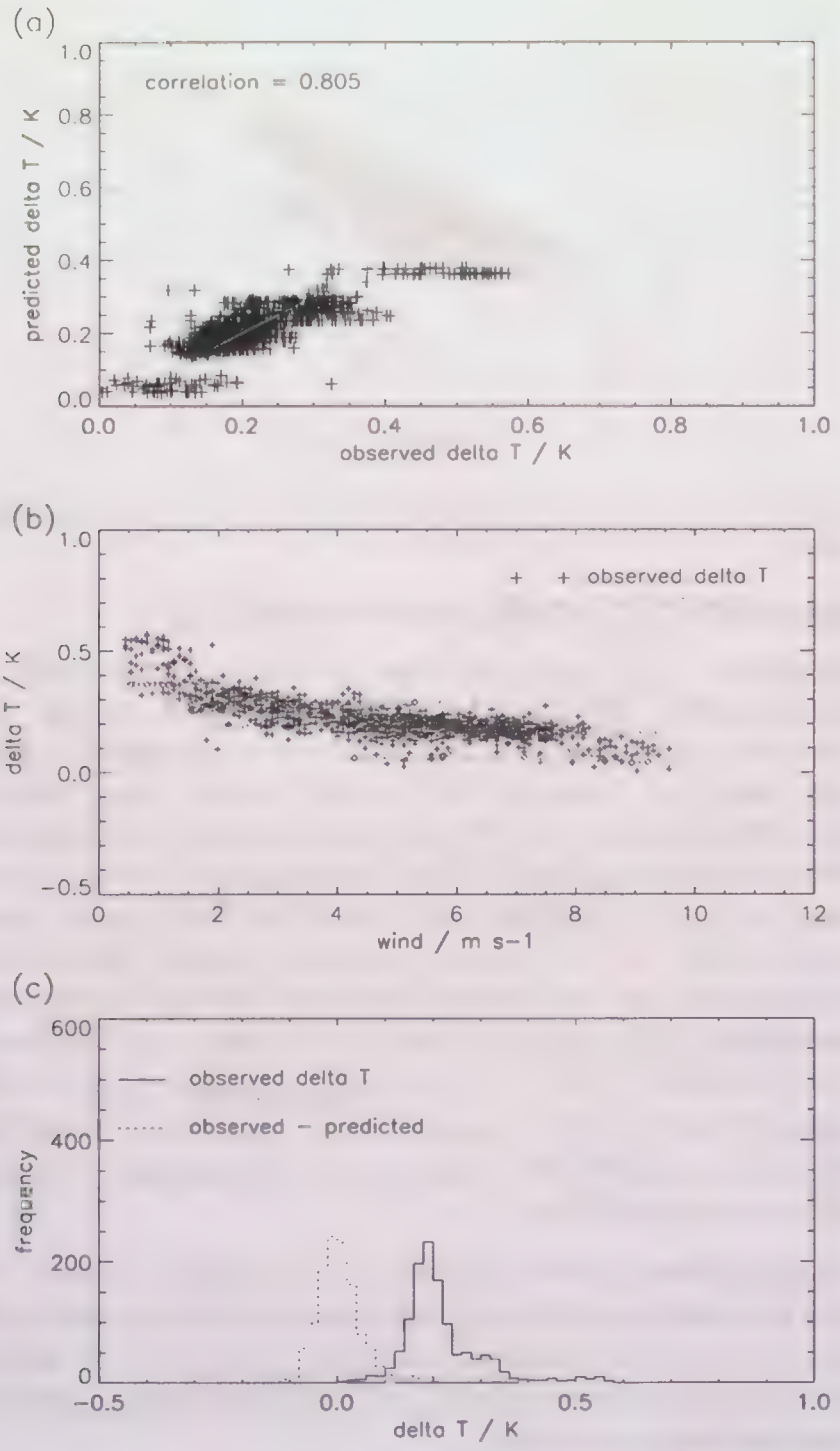

Figure 10: Predictions of ΔT using FA scheme, with λ_0 of 4.6. Scheme was forced by NWP model flux data, with correction applied to predicted ΔT as described in text. (a) predicted ΔT plotted against observed ΔT, in K; (b) ΔT plotted as a function of windspeed, observed values as black crosses and predicted values as grey open symbols; (c) histogram showing ΔT binned according to windspeed, with observed in solid black line, predicted in solid grey line, and δT_{o-p} in dotted black line.

Figure 11a shows the relationship between NWP model wind speed values and those measured in situ, both for a 10-m elevation. The lack of correspondence at the wind speed extremes is highlighted by the residuals plotted in Figure 11b. Values for u_* derived from the NWP flux data are therefore unrepresentative of the highest and lowest in situ values. Similarly, values for latent, sensible and long-wave heat fluxes

are also averages: the combined error from these sources propagates into the calculation of ΔT, and can be corrected for, at least in part, by a systematic offset.

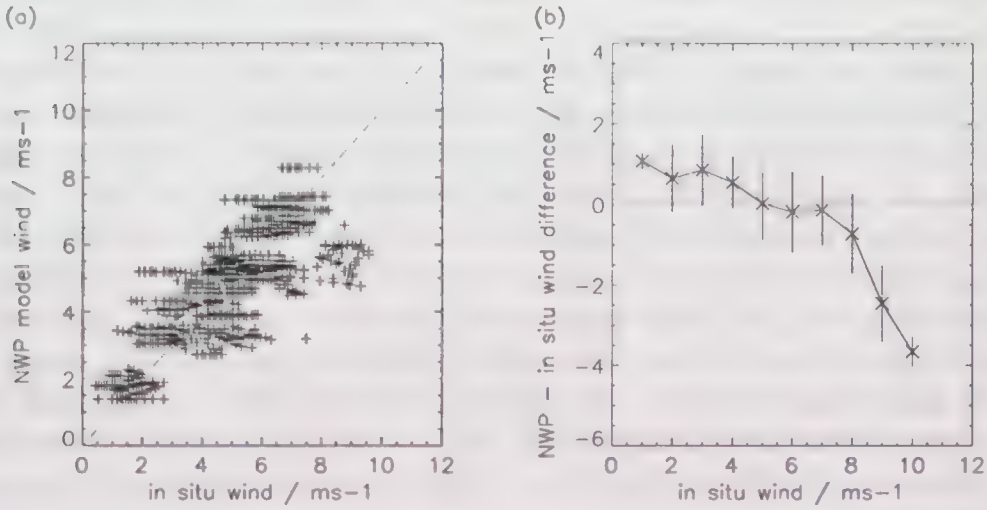

Figure 11: The relationship between wind speeds derived from NWP model analyses and those measured in situ. (a) direct comparison; (b) mean residuals (with error bars of $\pm 1\ \sigma$), against in situ wind speed.

5. Application to satellite data from ATSR-2

To investigate the application of a skin effect model in a processing scheme for satellite-derived SST measurements, we have used a set of collocated observations from ATSR-2 and buoys. ATSR-2 followed on from the first ATSR to complete a decadal record of highly accurate satellite-derived sea surface temperature data for climate research (Mutlow et al. 1999). The successful launch of a third instrument in the series, the Advanced ATSR (AATSR), on board the European Space Agency's Envisat platform in March 2002 means that this record will be continued and will become a valuable tool for climate monitoring purposes. The effective reconciliation of satellite-derived skin SSTs with in situ measurements is therefore an important step towards the goal of augmenting existing SST climate analyses. Previous comparisons between satellite-derived and in situ SSTs have focused either on validation of the ATSR instrument or on extending observational datasets (e.g., Merchant and Harris 1999; Murray et al. 2000); our intention is rather to test the global performance of a skin effect model.

The ATSR-2 data were provided by the ATSR team (reprocessed using v321 of their SADIST2 software, http://www.atsr.rl.ac.uk) as cloud-free top-of-atmosphere consolidated brightness temperatures in three thermal infrared channels (at 3.7, 10.8 and 12.0 μm) and in two views (nadir and forward) at 10 arcminute spatial resolution. Satellite data were matched to quality-controlled drifting and moored buoy observations received at the Met Office via the Global Telecommunications System (GTS) and also from the Tropical Atmosphere Ocean project (http://www.pmel.noaa.gov/tao/index.shtml). Buoy observations located within the 10 arcminute ATSR-2 cell and falling within a ±60 minute time window around the satellite observation were classified as good matchups. A total of 1243 night time matchups between June 1995 and June 1997 were obtained, and their global distribution is illustrated in Figure 12.

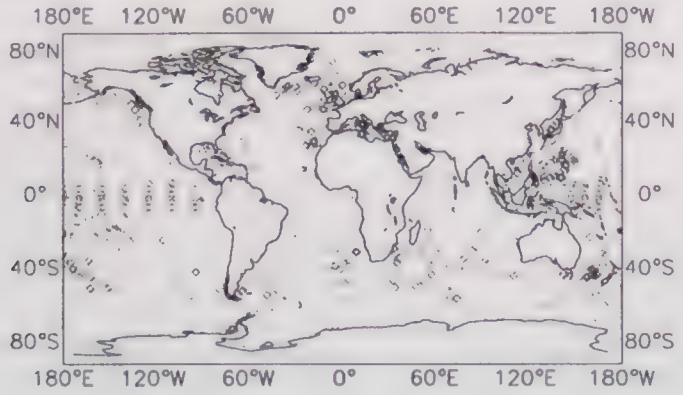

Figure 12: Distribution of 1243 night time collocations of buoy and ATSR-2 observations during June 1995 to June 1997.

Skin SSTs were derived from the ATSR-2 brightness temperature data following the retrieval scheme described most recently by Merchant et al. (1999). Aerosol-robust retrieval coefficients for ATSR-2 were derived by Chris Merchant (pers. comm., July 2000), and two different algorithms were applied. The first is the standard night time retrieval, "dual-3", and makes use of all six available brightness temperatures, from the

two views and three channels. The second, "dual-2" uses only the 10.8 and 12.0 μm channels, in both views: this is the standard retrieval available for day time observations when the 3.7 μm channel is contaminated by solar contributions.

Wind and heat flux data corresponding to the times and locations of the ATSR-2 observations were obtained from Met Office global NWP analyses, as described above. These data were used to derive estimates of the bulk–skin temperature difference predicted by the FA model. The FA model was applied using a λ_o value of 4.6 and predicted ΔT values were systematically adjusted by 0.04 K to account for flux errors, as above. Bulk–skin temperature differences from the buoy/satellite matchups were calculated as both buoy SST minus dual-3 skin SST, and buoy SST minus dual-2 skin SST. In order to minimise the mean δT_{o-p}, a constant offset term was applied to the satellite SSTs, if necessary. The data were binned according to wind speed, and means and standard errors are plotted in Figure 13.

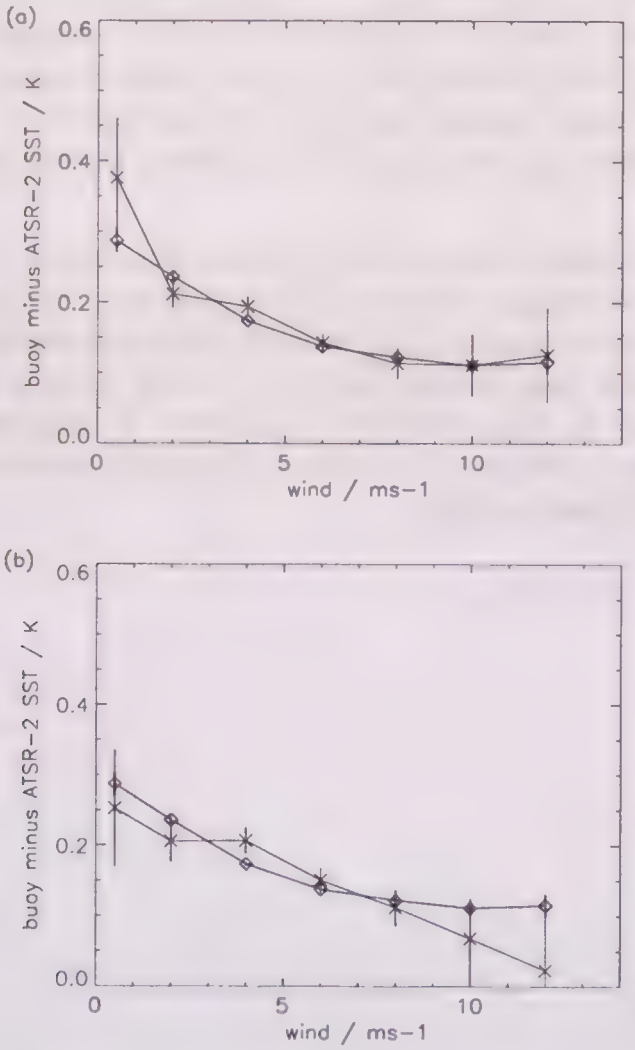

Figure 13: Difference of buoy-measured SST minus ATSR-2 derived SST against wind speed, shown in black as the mean value of a 2 ms^{-1} wind speed bin, marked with a cross, and standard error ($\sigma/\sqrt{N}$) bars. Grey line with diamonds shows bulk-skin temperature difference predicted from the Fairall model forced by NWP data matched to each satellite observation, and with λ_o of 4.6. (a) for retrievals using dual view and 3 channels; (b) for retrievals using dual view and 2 channels, and a constant offset of 0.018 K added to skin SSTs.

The buoy/satellite matchup data provide a trend of bulk–skin temperature difference against wind speed which is convincingly similar to that seen in the ship data (Figure 2). For ATSR-2 SSTs retrieved using the dual-3 algorithm (Figure 13a), the bulk-skin ΔT is successfully predicted by the FA model. There was no need to adjust the dual-3 SSTs to optimise the match between model and observed ΔT, as the mean $\delta T_{o\text{-}p}$ was negligible. It is only at the lowest wind speeds that the model appears to under predict the true buoy–satellite SST difference, and this is likely related to the use of averaged flux data.

Skin SSTs retrieved using the dual-2 algorithm (Figure 13b) are systematically cooler than those retrieved using dual-3, as has been noted elsewhere (Murray et al. 1998; Merchant and Harris 1999). An offset of 0.18 K was added to the dual-2 skin SSTs in order to obtain matching predictions from the skin effect model. The discrepancy between the two skin SST retrievals is related to inadequacies in radiative transfer modelling and a resultant lack of convergence between brightness temperatures modelled in all of the channels. Additionally, there is less absorption by water vapour at 3.7 μm than at 10.8 or 12 μm; this is especially significant over the tropics where atmospheric water vapour burdens are high. Overall, the dual-3 retrievals of SST appear more reliable since the observed skin effect corresponds well with that predicted.

The close match between observed and predicted bulk–skin temperature differences shown in Figure 13a indicates that the FA model produces reliable predictions on a global scale, as well as in the more limited region of the Western Pacific covered by the ship data in Section 4. Thus, at least for night time data, ATSR-2 skin SSTs could be reliably adjusted to an equivalent bulk temperature, in line with historic in situ measurements, by the systematic application of this scheme to every observation, using flux data from NWP model analyses.

6. Conclusions and implications

The night time skin-bulk SST data from the Nauru 1999 cruise were well described by an exponential dependence on wind speed. This empirical function assumes that ΔT is determined only by wind speed: for a spatially- and temporally-limited study where the net heat flux and wind speed follow a close relationship, this assumption is approximately true. However, for a globally appropriate conversion scheme, the effect of the net heat flux must be considered independently (e.g. Wick et al., 1996).

From the three parameterisations tested here, the approach developed by Fairall et al (1996a) provided the best prediction of ΔT across the wind speed range. Models based closely on surface renewal theory were unable to capture the trend observed at low wind speed. ΔT predicted using the Fairall et al (1996a) scheme could reliably be used to convert from satellite radiometric retrieval of skin SST to an equivalent bulk SST. Our results indicate that Met Office NWP model flux data are accurate enough to produce significant skill from the Fairall prediction scheme for the night-time cool skin, although higher quality predictions can be achieved by using in situ measurements of fluxes.

The ATSR series of satellite sensors has now provided more than 10 years of highly accurate global SST data, ripe for inclusion in climate variability studies. The AATSR will extend this unique record, with data available in near-real time for inclusion in SST analyses (e.g., Parker et al. 1999; Reynolds & Smith 1994). For satellite-derived SST data to be fully exploited, it will always be necessary to generate equivalence between these data and the historical set of ship and buoy measurements. An important first attempt at this process is to implement a parameterisation such as that by Fairall et al (1996a) for operational skin to bulk SST conversion. The global validity of this approach has been demonstrated in the above comparisons of SST derived from ATSR-2 data and measured by buoys.

Ultimately, blending of all kinds of in situ and satellite data for effective climate analysis should involve a scheme in which the depth of each SST measurement is explicitly accounted for. Until that time, the definition of bulk SST depth remains a difficulty. For the ship data used in this study, the schemes were tuned to correct an observed skin temperature to match a bulk temperature at a depth of 4.5 m. A satellite data correction scheme for operational use relies on a global buoy data set as representative of bulk SST, but as indicated here, tuning may be similar to that required for ship data sets.

This study has addressed only the skin effect encountered in night time SST data. A fully operational scheme must also address day time data and their associated complications. Since the parameterisations studied here have a fully physical basis, they can be extended to day time data, although the inclusion of solar warming in the skin layer may be necessary (e.g., Fairall et al., 1996a). A second problem for day time measurements is the potential for thermal stratification. Since diurnal warming at the ocean surface can produce skin temperatures several Kelvin warmer than the bulk temperature at a few metres depth (e.g., Webster et al., 1996), this problem is arguably of greater importance for an accurate climate record than that of the cool skin. However, its transient nature and gradual growth are much more difficult to predict,

and an accurate time history of heat fluxes and winds at the observation location from local dawn to observation time is required. A number of parameterisations applicable to the problem of diurnal warming have been suggested (e.g., Kraus and Turner 1967; Price et al. 1986; Kantha and Clayson 1994), but their utility for operational skin-bulk corrections may be limited by the accuracy and resolution of the flux data available as input to them.

Acknowledgements

This work was carried out in support of the Climate Prediction Programme, funded by the United Kingdom Department for Environment, Food and Rural Affairs (DEFRA). Tim Nightingale and the SISTeR instrument were funded by the U.K.'s Natural Environment Research Council ATSR-2 post-launch support programme. Ship data were collected on the *R/V Mirai* cruise MR99-K03 operated by the Japan Marine Science and Technology Center. We are grateful for buoy data provided by the TAO Project Office. ATSR-2 data are ©ESA/NERC/CCLRC: we thank Rutherford Appleton Laboratory for provision of the data used here, and Chris Merchant for provision of ATSR-2 SST retrieval coefficients.

References

Allen, M.R., Mutlow, C.T., Blumberg, G.M.C., Christy, J.R., McNider, R.T., and Llewellyn-Jones, D.T., 1994. Global change detection. *Nature* **370**, 24–25.

Barton, I.J., Prata, A.J., and Cechet, R.P., 1995. Validation of the ATSR in Australian waters. *J. Atmos. Ocean. Tech.* **12**, 290–300.

Cullen, M.J.P., 1993. The unified forecast/climate model. *Meteorol. Mag.* **122**, 81–94.

Donlon, C.J., and Nightingale, T.J., 2000. Effect of atmospheric radiance errors in radiometric sea-surface skin temperature measurements. *Appl. Optics* **39**, 2387–2392.

Donlon, C.J., and Robinson, I.S., 1997. Observations of the oceanic thermal skin in the Atlantic Ocean. *J. Geophys. Res.* **102**, 18585–18606.

Donlon, C.J., Nightingale, T., Fielder, L., Fisher, G., Baldwin, D., and Robinson, I.S., 1999. The calibration and intercalibration of sea-going infrared radiometer systems using a low cost blackbody cavity. *J. Atmos. Oceanic Technol.* **16** (9), 1183–1197.

Donlon, C.J., Minnett, P., Gentemann, C., Nightingale, T.J., Barton, I.J., Ward, B. and Murray, M.J., 2002. Toward improved validation of satellite sea surface skin temperature measurements for climate research. *J. Clim.* **15**, 353–369.

Fairall, C.W., Bradley, E.F., Godfrey, J.S., Wick, G.A., Edson, J.B., and Young, G.S., 1996a. Cool-skin and warm-layer effects on sea surface temperature. *J. Geophys. Res.* **101** (C1), 1295–1308.

Fairall, C.W., Bradley, E.F., Rogers, D.P., Edson, J.B., and Young, G.S., 1996b. Bulk parameterisation of air-sea fluxes for TOGA-COARE. *J. Geophys. Res.* **101**(C2), 3744–3764.

Harris, A. R., Merchant, C. J., Candy, B., Clayson, C.A., Murray, M.J., Zavody, A.M., and Allen, M.R., 1998. Satellite retrievals of sea surface temperature for long-term climate monitoring. In: Proceedings of 9th AMS Conference on satellite meteorology and oceanography, Paris, 162–165.

Hasse, L., 1963. On the cooling of the sea surface by evaporation and heat exchange. *Tellus* **15**, 363–366.

Hasse, L., 1971. The sea surface temperature deviation and the heat flow at the sea-air interface. *Boundary Layer Meteorol.* **1**, 368–379.

Kantha, L.H., and Clayson, C.A., 1994. An improved mixed layer model for geophysical applications. *J. Geophys. Res.* **99**(C12), 25235–25266.

Kearns, E.J., Hanafin, J.A., Evans, R.H., Minnett, P.J., and Brown, O.B., 2000. An independent assessment of pathfinder AVHRR sea surface temperature accuracy using the Marine Atmosphere Emitted Radiance Interferometer (MAERI). *Bull. Am. Meteorol. Soc.* **81**, 1525–1536.

Kraus, E., and Turner, S., 1967. A one-dimensional model of the seasonal thermocline: The general theory and its consequences. *Tellus* **19**, 98–106.

Kent, E.C., Forrester, T.N., and Taylor, P.K., 1996. A comparison of oceanic skin effect parameterizations using shipborne radiometer data. *J. Geophys. Res.* **101** (C7), 16,649–16,666.

Liu, W.T., and Businger, J.A., 1975. Temperature profile in the molecular sublayer near the interface of fluid in turbulent motion. *Geophys. Res. Lett.* **2**, 403–404.

Liu, W.T., Katsaros, K.B., and Businger, J.A., 1979. Bulk parameterization of air-sea exchanges of heat and water vapour including the molecular constraints at the interface. *J. Atmos. Sci.* **36**, 1722–1735.

Llewellyn-Jones, D.T., Minnett, P.J., Saunders, R.W., and Zavody, A.M., 1984. Satellite multichannel infrared measurements of sea surface temperature of the N.E. Atlantic Ocean using AVHRR/2. *Q. J. R. Meteorol. Soc.* **110**, 613–631.

McClain, E.P., Pichel, W.G., and Walton, C.C., 1985. Comparative performance of AVHRR-based multichannel sea surface temperatures. *J. Geophys. Res.* **90**, 11587–11601.

Merchant, C.J., Harris, A.R., Murray, M.J., and Zavody, A.M., 1999. Toward the elimination of bias in satellite retrievals of sea surface temperature 1. Theory, modeling and interalgorithm comparison. *J. Geophys. Res.* **104**(C10), 23565–23578.

Merchant, C.J., and Harris, A.R., 1999. Toward the elimination of bias in satellite retrievals of sea surface temperature 2. Comparison with in situ measurements. *J. Geophys. Res.* **104**(C10), 23579–23590.

Minnett, P.J., Knuteson, R.O., Best, F.A., Osborne, B.J., Hanafin, J.A., and Brown, O.B., 2001. The marine-atmospheric emitted radiance interferometer: A high-accuracy, seagoing infrared spectroradiometer. *J. Atmos. Ocean. Tech.* **18**, 994–1013.

Murray, M.J., Allen, M.R., Mutlow, C.T., Zavody, A.M., Jones, M.S., and Forrester, T.N., 1998. Actual and potential information in dual-view radiometric observations of sea surface temperature from ATSR. *J. Geophys. Res.* **103** (C4), 8153–8165.

Murray, M.J., Allen, M.R., Merchant, C.J., Harris, A.R., and Donlon, C.J., 2000. Direct observations of skin-bulk SST variability. *Geophys. Res. Lett.* **27**, 1171–1174.

Mutlow, C.T., Murray, M.J., Smith, D.L., Watts, P.D., and North, P., 1999. New data sets for climate change and land use studies are on track. *Eos, Transactions, AGU* **80** (49), 589, 594–595.

Parker, D.E., Rayner, N.A., Horton, E.B., and Folland, C.K., 1999. Development of the Hadley Centre sea ice and sea surface temperature data sets (HadISST). *WMO Workshop on Advances in Marine Climatology, CLIMAR99*, 194–203, (available from Environment Canada, Ontario).

Parker, D.E., Folland, C.K., and Jackson, M., 1995. Marine surface temperature: observed variations and data requirements. *Clim. Change* **31**, 559–600.

Pierson, W.J., 1978. Verification procedures for the Seasat measurements of the vector wind with the SASS. CUNY Institute of Marine and Atmospheric Sciences, City University, New York, contract number N00014-77-C-0206.

Price, J.F., Weller, R.A., and Pinkel, R., 1986. Diurnal cycling: Observations and models of the upper ocean response to diurnal heating, cooling and wind mixing. *J. Geophys. Res.* **91**, 8411–8427.

Reynolds, R.W. & Smith, T.M., 1994. Improved global sea surface temperature analyses using optimum interpolation. *J. Clim.* **7**, 929–948.

Robinson, I.S., Wells, N.C., and Charnock, H., 1984. The sea surface thermal boundary layer and its relevance to the measurement of sea surface temperature by airborne and spaceborne radiometers. *Int. J. Remote Sens.* **5**, 19–45.

Saunders, P.M., 1967. The temperature at the ocean-air interface. *J. Atmos. Sci.* **24**, 269–273.

Smith, R.N.B., and Williams, A., 2000. Subsurface, surface and boundary layer processes. *Unpublished. Unified Model documentation paper no. 24*, available on request from the Head of Climate Prediction, Met Office, London Road, Bracknell, RG12 2SZ, UK.

Smith, S. D., 1988. Coefficients for sea surface wind stress, heat flux and wind profiles as a function of wind speed and temperature. *J. Geophys. Res.* **93**,15467–15474.

Soloviev, A.V. and Schlüssel, P., 1994. Parameterization of the cool skin of the ocean and of the air-ocean gas transfer on the basis of modeling surface renewal. *J. Phys. Oceanogr.* **24**, 1339–1346.

Walton, C.C., Pichel, W.G., Sapper, J.F., and May, D.A., 1998. The development and operational application of nonlinear algorithms for the measurement of sea surface temperatures with the NOAA polar-orbiting environmental satellites. *J. Geophys. Res.* **103**(C12), 27999–28012.

Webster, P.J., Clayson, C.A., and Curry, J.A., 1996. Clouds, radiation, and the diurnal cycle of SST in the tropical Western Pacific. *J. Clim.* **9**, 1712–1730.

Wick, G.A., Emery, W.J., Kantha, L.H., and Schlüssel, P., 1996. The behavior of the bulk-skin sea surface temperature difference under varying wind speed and heat flux. *J. Phys. Oceanogr.* **26**, 1969–1988.

Závody, A.M., Mutlow, C.T., and Llewellyn-Jones, D.T., 1995. A radiative transfer model for sea surface temperature retrieval for the along-track scanning radiometer. *J. Geophys. Res.* **100**, 937–952.